

UNIVERSITY OF TWENTE
FACULTY OF ENGINEERING TECHNOLOGY
SOFT ROBOTICS LAB

Designing a soft sensory actuator for minimally invasive surgery with the focus on sensor behaviour

E.A. Veuger

Committee:

Dr. A. Sadeghi (Ali)

Ir. N. Willemstein (Nick)

Dr. I. Tamadon (Izad)

BSc Thesis Biomedical Technology

February 29, 2024

Abstract

Minimal invasive surgeries(MIS) using an endoscope are becoming more popular compared to their traditional open surgeries. A disadvantage of MIS is a limited working area, because of their rigidness. The field of soft robotics focuses on tackling this hurdle. Composing the end of the endoscope of soft material will increase the flexibility of the endoscope. Resulting in an increased reaching capacity of the endoscope.

In this study, the actuator is fabricated of Ecoflex 00-10. Incorporating three fiber reinforced inflatable balloons into the actuator allows for controllable movement. Subsequently, adding sensors allows for the measurement of these movements. Two consecutive modules are placed in series to create an S-shape.

The results compare a conductive rubber and a water with salt sensor. From the tests can be concluded that conductive rubber gave the most stable results over time. Accordingly, this is used as a sensor in the modules, every module has three sensors. To confirm the usability, different parameters are evaluated. The resistance, pressure, and radius of the sensor provide this information. The radius is measured using computer-vision technology. The results showed an increased pressure leads to a resistance change. Moreover, as the radius of the actuator was found to decrease, the actuator would be deformed.

Samenvatting

Minimaal invasieve operaties(MIO) worden steeds populairder ten opzichte van hun gebruikelijke open operaties. Het nadeel van MIO is dat een endoscoop niet altijd alle delen van het lichaam kan bereiken, omdat ze van harde materialen zijn. Zachte robotica kan hiervoor een oplossing zijn. door de endoscoop van zacht materiaal te maken wordt deze flexibeler. Hierdoor kan de endoscoop meer punten bereiken.

In deze studie is een actuator van Ecoflex 00-10 gemaakt. Hierin zijn drie vezel versterkte ballonnen geplaatst om de actuator te laten bewegen. Vervolgens zijn er sensoren toegevoegd om de beweging te meten. Twee modules zijn achter elkaar geplaatst om een S-vorm te kunnen maken.

De resultaten vergelijken weerstand geleidbaar rubber en water met zout als sensoren. Hieruit is geconcludeerd dat geleidbaar rubber de meest stabiele resultaten over tijd geeft. Vervolgens is dit gebruikt als sensor in de module, elke module heeft drie sensoren. Om de bruikbaarheid van de sensor te testen zijn de weerstand, druk en straal van de sensor gemeten. De straal is bepaald door middel van computervision technologie. De resultaten laten zien dat bij een verhoogde druk de weerstand verandert. Daarnaast wordt de straal van de actuator kleiner, de actuator vervormd dus.

Contents

1	Introduction	3
2	Materials and method	5
2.1	Design	5
2.2	Fabrication	5
2.3	Sensor test protocol	6
2.4	Sensorized actuator characterization	7
2.4.1	Full actuator sensor characterization	7
3	Results and discussion	8
3.1	Sensor tests	8
3.1.1	Water with salt 100g/L	9
3.1.2	Water with salt 200g/L	10
3.1.3	Conductive rubber	11
3.1.4	Sensor behaviour over time	12
3.2	Sensorized actuator characterization	12
3.3	Sensor characterization full actuator	15
4	Conclusion	16
	Bibliography	18
A	Extra figures fabrication and setup	21
B	First mold design	22
C	Results resistance and pressure over time	23

1 Introduction

For many abdominal procedures, minimally invasive surgeries(MIS) are becoming the norm instead of an open surgical approach [1, 2]. MIS aims to reduce tissue damage during the intervention and speed up the recovery. In the United States, the amount of MIS increased from 8.9% in 1993 to 20.7% in 2014 [3]. The benefits are reduced pain, quicker return of oral intake, shorter hospitalization, improved cosmetic results, and decreased morbidity [2, 4]. Moreover, the MIS approach tends to be less expensive than open surgery, for the hospital. [5]. However, there are also several problems for the clinician including, a reduced degree of freedom, lack of visibility, lack of direct access to the surgical area, and a relatively high chance of damaging other tissue due to the instrument traveling through the body [6, 7].

In MIS often an endoscope is used, every application has a different device, often named after the target organ. When going in the body via the mouth or anus it is mostly called endoscopic surgery, while when using an artificial opening there will be referred to as a laparoscopic surgery. An endoscope is often composed of different sensors and tools, they are a few millimeters thick. Some endoscopes are more flexible, while others are more rigid. The disadvantage of a more flexible endoscope is that it may lack the force and stability that normal rigid tools would provide [8]. A way to make endoscopes more flexible can be by making them out of soft materials, which is done in the field of soft robotics.

As a result of using softer materials, soft robots can sometimes reach more points in the human body. Their softness allows for more flexibility and for easier moving past and around organs. Because of this, they can have different or more applications than rigid robots. In Figure 1, the possible advantages of a soft robot are compared to a rigid instrument. The rigid laparoscopy has four degrees of freedom(DOF), when organs are present between the target point and the entry point the workspace of the tool is limited [7]. Poor maneuverability is also confirmed by clinicians using these tools [9]. An instrument with more DOFs can be a solution, also shown in Figure 1. A more flexible instrument can move around the organs and so reach the target point. Flexible actuators are created to make new tools for traditional applications [10].

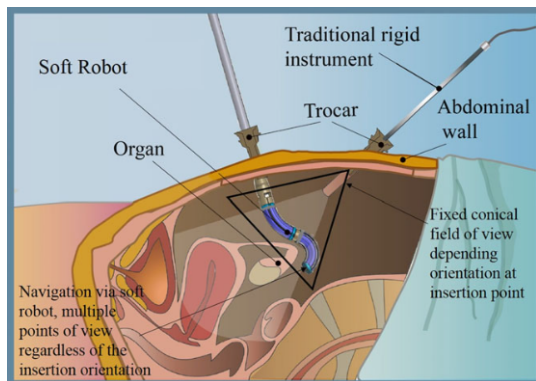


Figure 1: Illustration of a soft device and a rigid instrument in the human body [7]

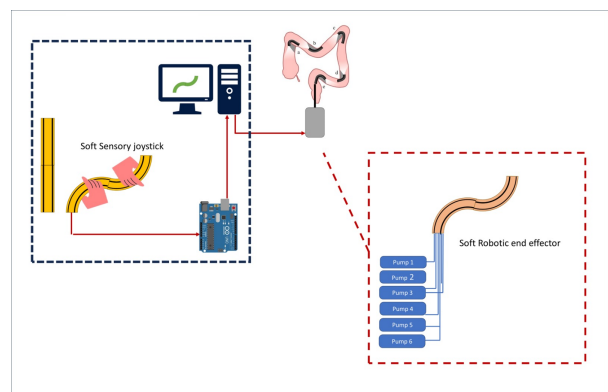


Figure 2: Visualization of future application

In Figure 2, a visualization is seen of the possibilities of a soft endoscope. On the right side, the soft endoscope embedded with sensors and actuated by pumps is shown. This endoscope could be controlled by a clinician with a joystick. The joystick has sensors, which values are transmitted to an intermediate medium. These are converted and the endoscope will form in the same shape as the joystick. Both the actuator and the joystick consist of two modules and are able to form an S-shape.

An actuator is responsible for the moving of the robot. This requires control signals and an energy source. In soft robotics, different designs are available. Generally, two types of fluidic actuators are used. Firstly there are pneumatic networks(PneuNet actuator), these actuators consist of an elastomer and are designed with channels and chambers, an example is shown in Figure 3 [11]. The channels can be inflated by adding pressure, resulting in a motion. By changing the wall thickness, the geometry of the chambers, and using different materials, the form of expansion can be influenced. The actuator will expand in the least stiff regions. A more elastic material will expand more than a rigid material, resulting in the bending of the actuator [12]. With these actuators complex motions can be achieved [13].

Another class of soft actuators are fiber-reinforced actuators. The concept of this is an elastomer base wrapped with inextensible fiber reinforcements or layers. When inflated, the elastomer bladder expands in all directions, like a balloon. Wrapping in fibers prevents the elastomer from expanding in the radial direction. A strain-limiting layer of inextensible material can also be added, this constrains it from expanding in the region of the layer. If the actuator is now inflated, it will bend [12, 14].

With fiber-reinforced actuators, a wider range of motion can be achieved. Moreover, they have smaller end caps with a smaller seam area than PneuNets, which have a seam area around the whole base layer. This increases the risk of delamination failure for the PneuNets. However, making fiber-reinforced actuators is more time-consuming and more materials are necessary, it can take up to five days, while PneuNets can be made in an hour [12].

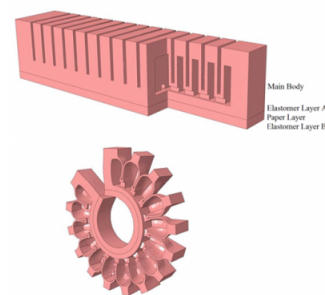


Figure 3: PneuNet actuator [11]

The motion of the fiber-reinforced actuator is determined by axial and radial expansion and can be affected by applying a strain-limiting layer and fiber reinforcement in different configurations. Four different types of motions can be defined; bending, twisting, expansion and extension [15].

The bending motion can be achieved by wrapping the fiber in a symmetrical, double-helix configuration and a strain-limiting layer can be added. Now the actuator only expands axially on one side and thus bends.

Extension of the actuator can be achieved by wrapping the fiber similar to the bending motion, a double helix configuration, but without a strain-limiting layer. When inflated, the actuator expands in the axial direction.

Twisting of the actuator can be achieved by wrapping the fiber in a single helical configuration. Due to the twisting, the number of coils is reduced, and the diameter of the helix is increased.

These three types of motions can also be combined by placing multiple actuators in series, shown in Figure 4.

The amount of bending and pressure necessary can be influenced by the spacing of fiber wrapping. When the turn number is increased, lower pressure is needed to achieve the same amount of bending. Decreasing the turn number too much, the fibers are spaced far apart, will result in bulging and radial expansion in between the fiber threads [12].

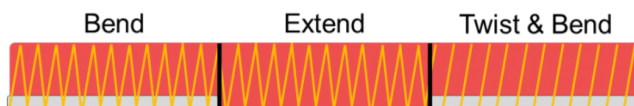


Figure 4: Illustration of different configurations of the strain-limiting components [12]

An example of a soft actuator designed for use in MIS is the STIFF FLOP [16]. The actuator is mostly made of elastomer. The actuator has three chambers for actuation and one central channel for granular jamming, the design is shown in Figure 5. The module is surrounded by a braided structure in bellow configuration, to limit the radial expansion of the module. Fras et al. [17] created a STIFF FLOP module with a new design for the chambers. Each chamber is fiber reinforced, instead of the older design where the whole module is reinforced. Consequently, an increased bending angle could be achieved.

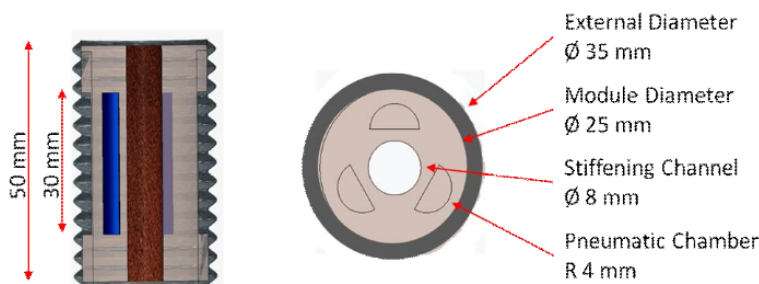


Figure 5: STIFF FLOP design [16]

To measure the movement of the actuator, it is necessary to use sensors. In a design like a STIFF FLOP, sensors should be more flexible, for which there is a growing demand [18]. Different sensor options are tested and embedded using the STIFF FLOP design. For example, Noh et al. [19] designed a force sensor using optical fibers. Truby et al. [20] created a sensor skin, based on kirigami, using conductive silicon sheets. These were placed around the actuator. Conductive elastomers are an example of stretchable and conductive materials. To make the elastomer conductive silver particles or carbon black can be used [21]. Several studies explored the use of carbon black, the conductivity of the material was low, but the loading level was also low. However, the mechanical and electrical properties after 100 strain cycles did only show a little degradation [22, 23]. Conductive rubber is a piezoresistive sensor, which changes resistance when a load or force is applied. Other options that could be explored are liquid sensors, an advantage is that they can move along with the actuator.

This study focuses on testing sensors and implementing sensors in a soft actuator. The sensor should be flexible and move with the actuator. The design of the actuator can be partially based on the STIFF FLOP design, using fiber reinforced balloons. The actuator requires 6 DOFs and be able to form an S-shape. The next section details the design and fabrication of the actuator and its test protocol. Next, the results are discussed, concluding with the recommendations and conclusion.

2 Materials and method

2.1 Design

An actuator for MIS is designed. It is required to be able to form an S-shape. Besides, it is made of soft material and sensors are embedded. The design was based on the STIFF FLOP. The actuator consists of two modules so that in the future when a joystick is also made with two modules these can be connected. Two modules, shown in Figure 6 are made and placed in series. The modules have an equal height of 80mm . In each module, three fiber reinforced balloons with a diameter of 12mm are placed. Each balloon is fiber reinforced in a single helical configuration. In both modules, there are three sensor channels with a 2mm diameter. The plastic air tubes for inflating the chambers are connected at the top of the upper module and the bottom of the lower module. In the middle gap of 8mm the plastic tubes from the upper three chambers run down. In addition, the copper wiring of the upper three sensors and the copper wiring of the ground connections of all sensors also run down here. The copper wires also ensure that the module does not extend.

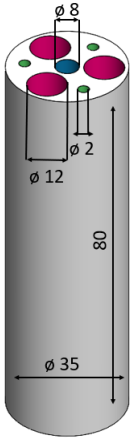


Figure 6: Prototype visualization in Solidworks, all dimensions in mm

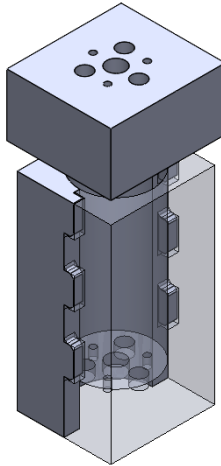


Figure 7: Mold to make the actuator

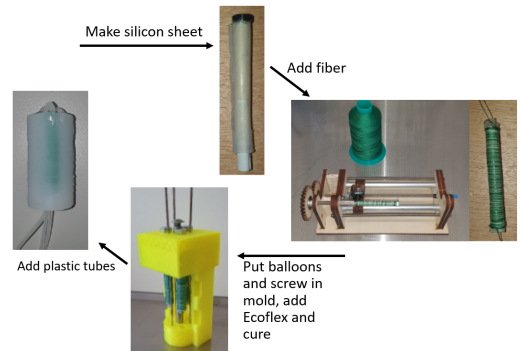


Figure 8: Overview of the fabrication process

2.2 Fabrication

The actuator is fabricated using Ecoflex 00-10 (Smooth-On Inc., United States). It is a silicon rubber which is often a two-part polymer. In its uncured state, it is liquid or gel. When adding both parts together, the material cures into an elastomer. The two parts need to be mixed in the same ratio and then cured for at least four hours at room temperature or 30 minutes at 70°C .

An overview of the fabrication process is shown in Figure 8. The fiber reinforced balloons are made from Ecoflex 00-10. First, a thin silicon sheet on a metal plate, of about $1mm$ is made. Paper is wrapped around a screw and tightened with paper tape, around this the silicon is wrapped and glued together with Ecoflex 00-10 again. When cured the fiber is wrapped around the balloon, and Ecoflex 00-10 is used to stick the fibers to the balloon. In Figure A.1 and A.2 the fiber reinforced balloon, a balloon wrapped around a screw, and the tool used for the fiber reinforcements are shown.

The actuator is made using a mold, shown in Figure 7 It consists of two base parts, Figure A.3a and A.3b and a cap, Figure A.3c. The mold is 3D-printed from PolyLactic Acid (PLA), using a $0.4mm$ nozzle, 20% infill and, a $0.8mm$ layer height. Before adding silicon to the mold, three balloons, three metal pins of $2mm$ diameter, and an $8mm$ pin are placed in the cap, shown in Figure A.5. After this, Ecoflex 00-10 is added to the mold and is cured for at least four hours. Lastly, the plastic tubes are glued with Sil-Poxy(Smooth-On Inc., United States) and Ecoflex 00-10. They are glued to the bottom of the lower module, and the top of the upper module. In Figure A.6 the result of this step is shown.

There will be tested different sensors, which will be explained in more detail later. Eventually, conductive rubber sensors made from TC7OEX-BLCKpellets(KraiburgTPE, Germany) are used. The sensors have a diameter of $0,6mm$. They are covered with Ecoflex 00-10 and then put through the $2mm$ sensor holes in the module. Next, the conductive rubber is soldered to copper wires using conductive rubber as soldering material. On one side all the sensors are connected to the ground wire, on the other side the other connections are soldered. When this is done, two modules can be connected using Ecoflex 00-10, and the mold shown in Figure A.4.

2.3 Sensor test protocol

To measure the performance of the actuator, water with salt, and conductive rubber are explored for use as a sensor in the module. The advantage of water with salt is that it is liquid, so it can form with the movements of the module, the resistance will change as the actuator deforms. The conductive rubber only changes resistance when it is stretched. The resistance of a material depends on four factors, see Formula 1. Here $R(\Omega)$ is the resistance, $\rho(\Omega m)$ is a material constant for the resistivity, $l(m)$ is the length of the conductor, and $A(m^2)$ is the area of the conductor.

$$R = \frac{\rho \cdot l}{A} \quad (1)$$

The resistance of a sensor can be measured with a voltage divider. A circuit diagram is in Figure 9a, Equation 2 is the belonging comparison. For $S_1(\Omega)$, a known resistance in the range of the sensor resistance is used. In this study for water and salt a $1k\Omega$ resistor is used, for the conductive rubber a resistor of $1.2M\Omega$ is used. $V_{in}(V)$ and $S_1(\Omega)$ are known and $V_{out}(V)$ can be measured. Solving for $S_2(\Omega)$, results in Equation 3. In this way, the resistance of the sensor can be determined.

$$V_{out} = \frac{S_2}{S_1 + S_2} \cdot V_{in} \quad (2)$$

$$S_2 = \frac{V_{out} \cdot S_1}{V_{in} - V_{out}} \quad (3)$$

Conductive rubber, water with $100g/L$ salt, and water with $200g/L$ salt are tested. All sensors are $60mm$ long, the conductive rubber has a diameter of $0.6mm$, and the salt solution is put in a tube with a diameter of $4mm$. The setup is seen in Figure 9. The tests are executed according to the following protocol.

1. Prepare the setup as described in the above section. Steps 2 to 5 should be done for 40 seconds.
2. Hold the sensor straight for 10 seconds, then bend the sensor for 10 seconds.
3. Hold the sensor straight for 10 seconds, then stretch it for 10 seconds.
4. Bend the sensor for 10 seconds, then stretch while bending it for 10 seconds.
5. While the sensor is stretched, straighten it for 10 seconds, then bend it for 10 seconds.
6. Leave the sensor on the surface for at least 5 minutes.

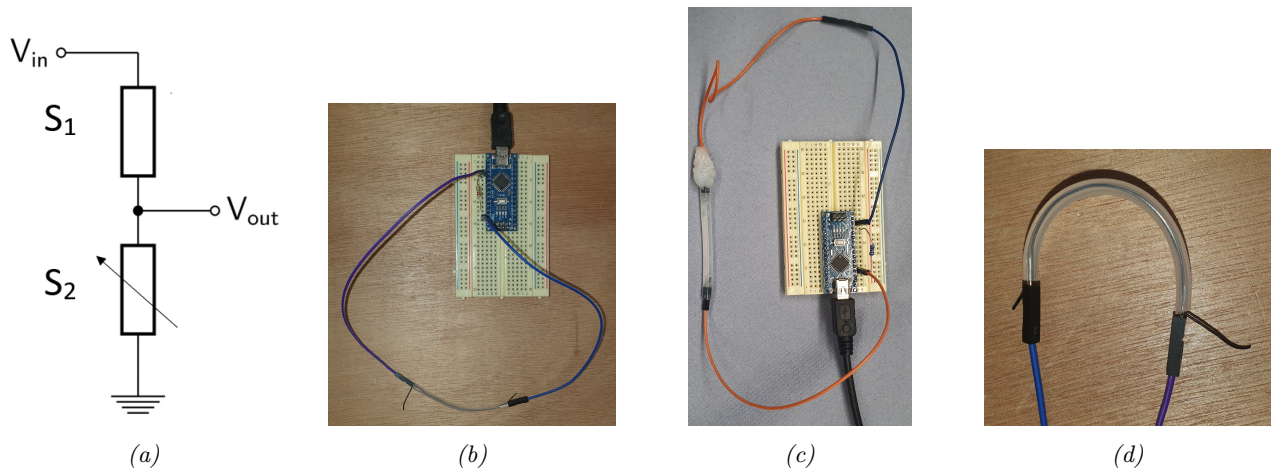


Figure 9: (a) circuit diagram of a voltage divider, (b) setup for testing conductive rubber, (c) setup for testing water with salt, (d) example of the bending angle

2.4 Sensorized actuator characterization

The goal of this experiment is to gain insight into the bending of the actuator versus the resistance of the sensors and the added pressure. The best-performing sensor is embedded in the actuator. The pressure was read by an Arduino Nano using an MPX5100DP(NXP Semiconductors, The Netherlands) pressure sensor. In Figure 10, the schematic setup is shown. Figure A.7 shows a picture of the setup. The camera is placed on a tripod. The actuator is connected to the Arduino and the syringe. On the actuator, three black dots are made using Ecoflex 00-10 mixed with black silicon pigment(Resion, Resintechnology). A white background is used to secure a good contrast with the black dots. This contrast is necessary to evaluate the video using computer vision technology in MATLAB. The following protocol is used.

1. Start the video and record the data with the Arduino.
2. Add pressure to the chamber until no further possible, while ensuring it does not fail.
3. Hold the pressure for 10 seconds and then release it.
4. Repeat the above steps for each single chamber. Thereafter connect two chambers to the syringe and repeat the procedure.

2.4.1 Full actuator sensor characterization

Lastly, the sensors are evaluated when two modules are placed in series. The sensor data is recorded, but there is no video made. Moreover, the actuator is moved by hand so the pressure data is not recorded. While testing, the configuration of the actuator is adjusted every ten seconds. The configurations are shown in Figure 11.

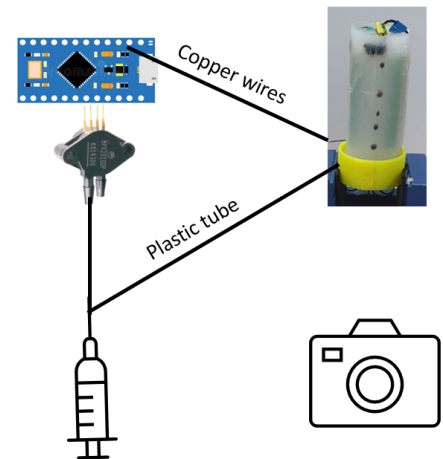


Figure 10: Schematic setup of the video analysis

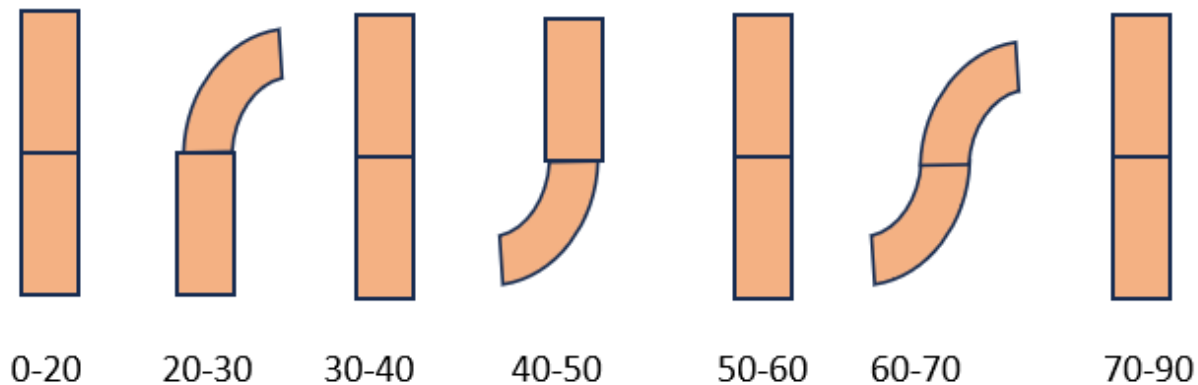


Figure 11: Protocol to test the sensorized actuator, time in seconds.

3 Results and discussion

3.1 Sensor tests

In this section, the results are shown from the experiments using the protocol as described in Section 2.3. Every ten seconds the sensors are in another configuration to test whether the resistance changes when the configuration of the sensors changes. The protocol is executed with water with salt $100g/L$, water with salt $200g/L$ and conductive rubber.

3.1.1 Water with salt 100g/L

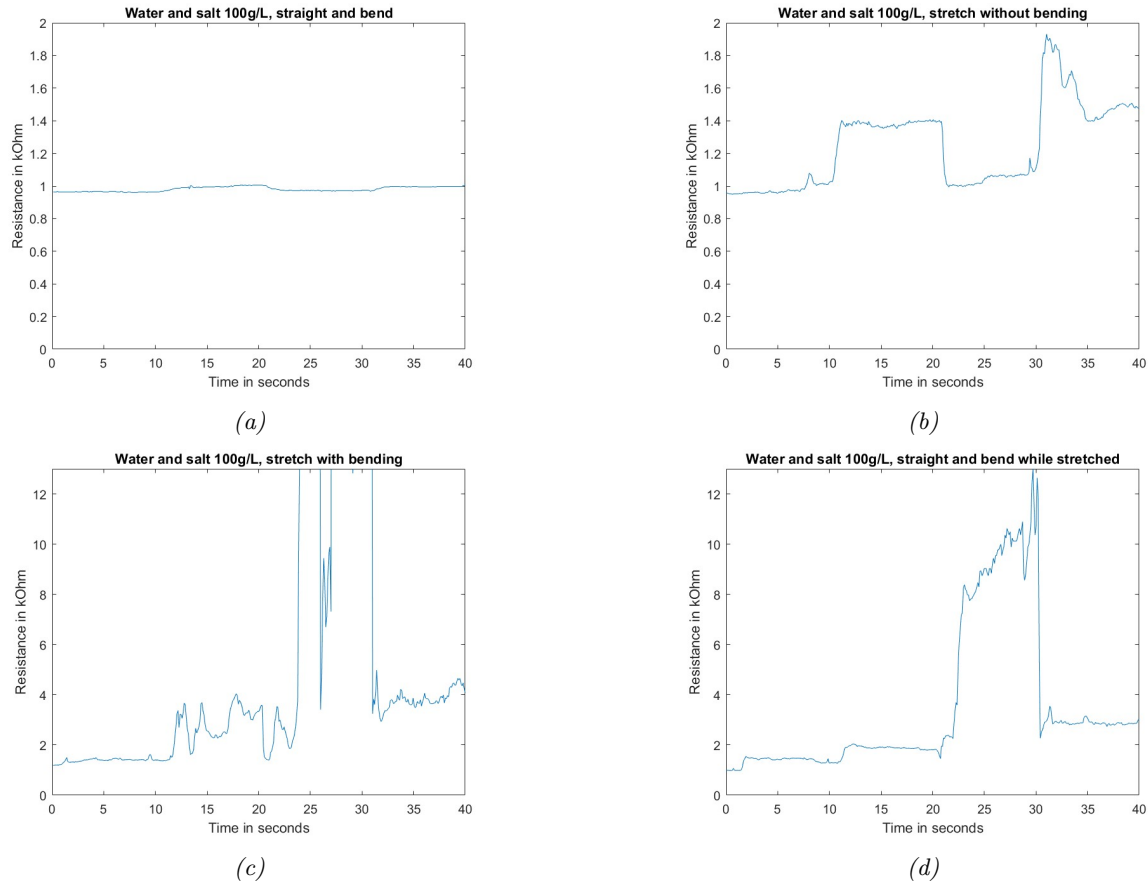


Figure 12: Test results water and salt 100g/L, (a) Straight and bend, (b) Straight and straight stretched, (c) Bend and bend stretched, (d) Straight stretched and bend stretched

Figure 12 illustrates the outcomes of using water and salt 100g/L as a sensor. When the configuration of the sensor changes a change in resistance is expected. Figure 12a shows a slight change in resistance between a straight and bent sensor. When stretching the sensor the resistance change is much bigger, this is shown in Figure 12b. Figure 12c and 12d both show resistance changes between different configurations. Furthermore, in both graphs, between 20 and 30 seconds, the resistance is considerably higher than in the first seconds. Reasons for this can be a loss of pin connection, water that leaked, or bubbles that obstructed the connection. In Figure 9c these bubbles are visible.

3.1.2 Water with salt 200g/L

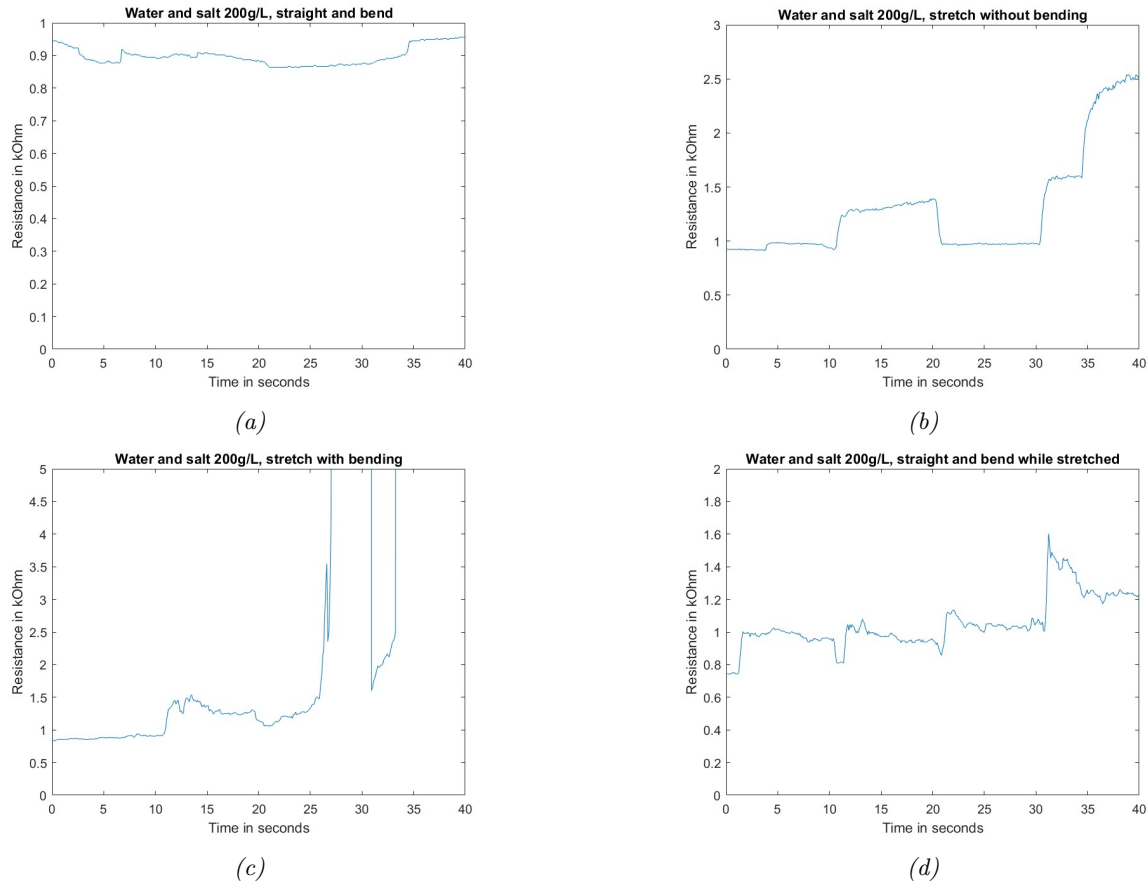


Figure 13: Test results water and salt 200g/L, (a) Straight and bend, (b) Straight and straight stretched, (c) Bend and bend stretched, (d) Straight stretched and bend stretched

In Figure 13, the results obtained from testing water and salt 200 g/L are shown. All Figures show a resistance change between configuration changes. In Figure 13b, in the last five seconds, the resistance rises. Furthermore, in Figure 13c the connection is lost after 25 seconds. Reasons for these high resistances can be a connection loss of the pins, or bubbles that obstructed the connection. In Figure 13d only in the last ten seconds a clear difference in resistance is visible. Comparing the results of both salt concentrations it can be noted the resistance values are similar. It would be expected the more salt is added the resistance decreases. However, this is not visible in these results. Potentially this only yields for lower salt concentrations, and in this case the concentration is too high so it does not apply anymore.

3.1.3 Conductive rubber

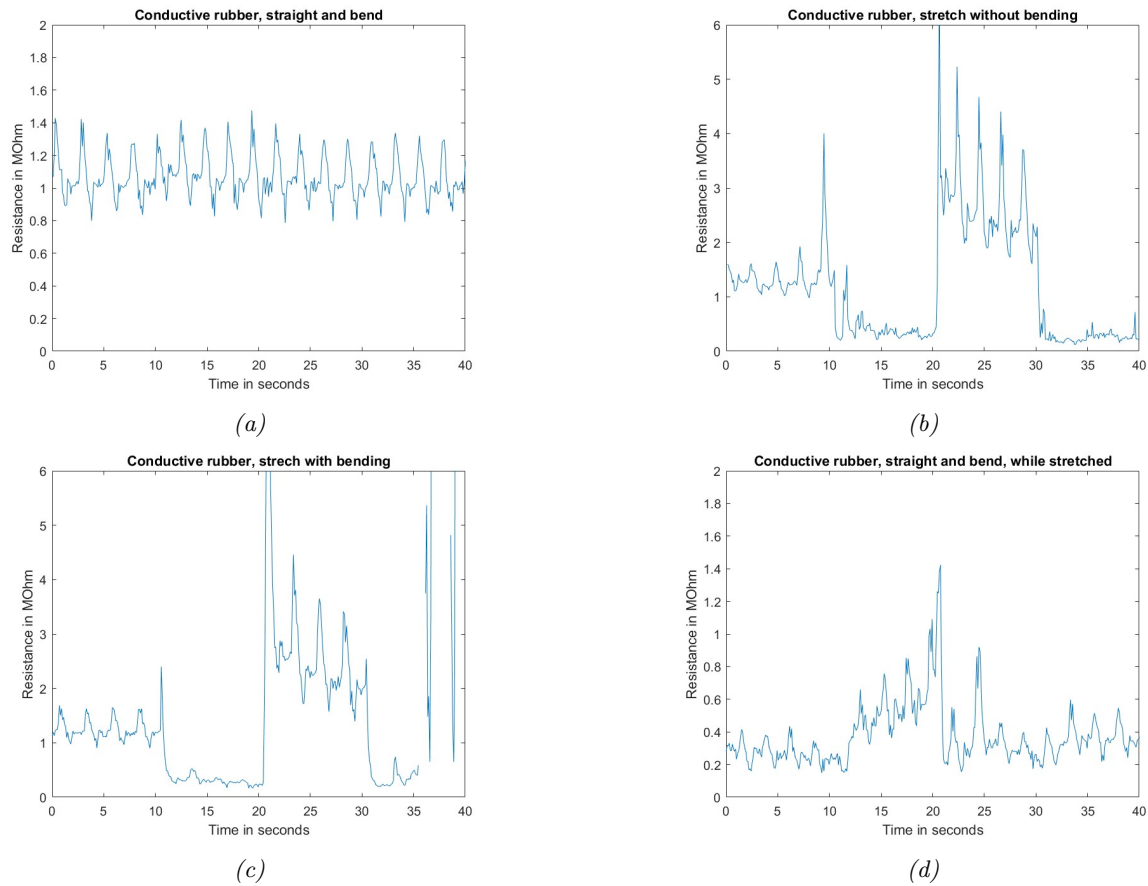


Figure 14: Test results conductive rubber, (a) Straight and bend, (b) Straight and straight stretched, (c) Bend and bend stretched, (d) Straight stretched and bend stretched

The resistance measurements of conductive rubber are shown in Figure 14. Notable is that the resistance oscillates, while that of water with salt does not. In Figure 14a, it can be seen that the resistance of conductive rubber oscillates around the $1.2M\Omega$. The oscillation is constant over time, so there cannot be seen a resistance change for a straight and bent sensor. A reason for this could be that the sensor is not fixed in the plastic tube. Consequently, the sensor can move in the tube and when the sensor is bent there is no change in stretching of the sensor. When the sensor does not stretch there is no change of measured resistance. For all three sensors applies that when the sensor is straight and then bent there is almost no difference in resistance visible, Figures 12a, 13a and, 14a.

A resistance change for a straight and a straight stretched sensor is shown in Figure 14b. Also in Figure 14c, a change is visible. When stretched, the resistance decreases as reduces the oscillation. At 20 seconds the sensor is in the bend configuration again, the resistance has to stabilize and is much higher than from zero to ten seconds. In the last ten seconds of Figure 14c, the connection between the pins is lost.

The difference in resistance between a bend and straight sensor, while stretched, is shown in Figure 14d. The difference between the first and second ten seconds is visible, while in the last 20 seconds, the resistance change is much smaller. A reason for this can be that the stretching was not well executed.

3.1.4 Sensor behaviour over time

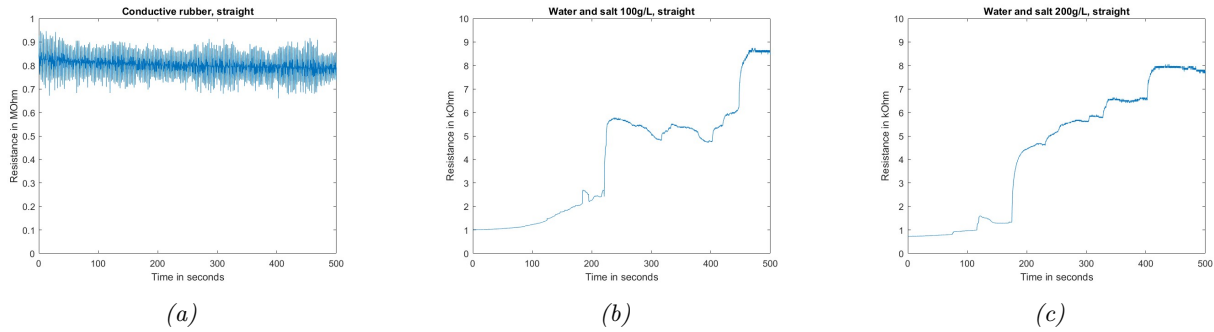


Figure 15: Test results straight sensor for 500 seconds, (a) Conductive rubber, (b) Water and salt 100g/L, (c) Water and salt 200g/L

In Figure 15, the results of letting the sensor lay down for 500 seconds are shown. It is expected that the resistance does not change over time. Visible is that the resistance of conductive rubber is much higher than that of water and salt. Furthermore Figure 15b and 15c show an increasing the resistance of water with salt. On the contrary, the resistance of conductive rubber, shown in Figure 15a, is constant over time but does oscillate. A reason for the increasing resistance is electrolysis. This causes bubbles to form in the water, visible in Figure 9c. These bubbles obstruct the connection between the water and the connection pins. These bubbles influenced all the test results of the water sensor. The resistance of conductive rubber is in a higher range than that of water with salt. Consequently, the resistance measurements of conductive rubber are less accurate.

All sensors show a change in resistance in different configurations, this is seen the best in Figures 12b, 13b, and 14b. When using water with salt as a sensor bubbles form, which leads to higher resistances and contact loss. Therefore, the resistance changes over time and the results are less reliable compared to the resistance change conductive rubber. Conductive rubber does show a stable resistance over time. Consequently, conductive rubber is chosen to use as a sensor in the modules.

For all results where the sensor needed to be bent and stretched at the same time applies that these results were less reliable. The stretching and bending at the same time were hard to execute, and so the amount of stretching was different every time. Moreover, for all results applied the stretching and bending were done by hand. This may have influenced the test results. Furthermore, it decreases the reproducibility of the experiment. Nevertheless, is it visible that when the sensor was stretched the resistance changed. So the experiment is sufficient to test if a resistance change is visible and which sensor is the best option to use. Several times the wires lost connection or the water leaked, which resulted in high resistances, visible in Figure 14c, 12c and 13c. When repeating this test it is recommended to make sure the connections are more stable. Moreover, it is recommended to stretch and bend the sensor in the same way the whole time to make sure all results are better comparable. Also, the conductive rubber should be stuck in the plastic tube to make sure it cannot move.

3.2 Sensorized actuator characterization

In this section, the results of the sensor and video analysis of the actuator are shown. In Figure 16 snapshots of the video are shown. The snapshots were made when the bending angle was maximum. Three videos were analyzed, the first two videos are when one chamber is inflated. In the third video, two chambers are inflated at the same time. When the pressure is increased it is expected to see a resistance change and a decreased radius.

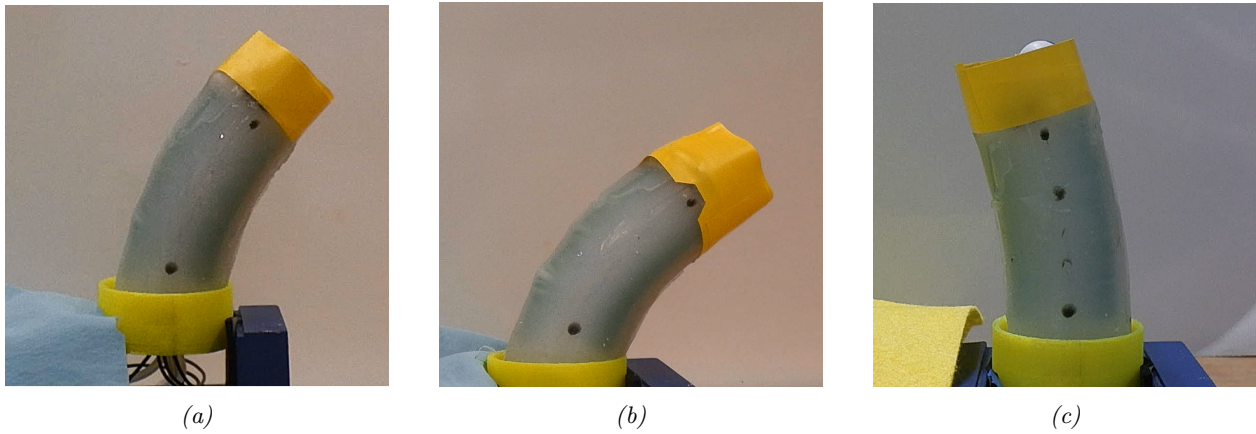


Figure 16: Snapshot of the video where maximum bending is reached (a) at 27 seconds, (b) at 15 seconds, (c) at 10 seconds

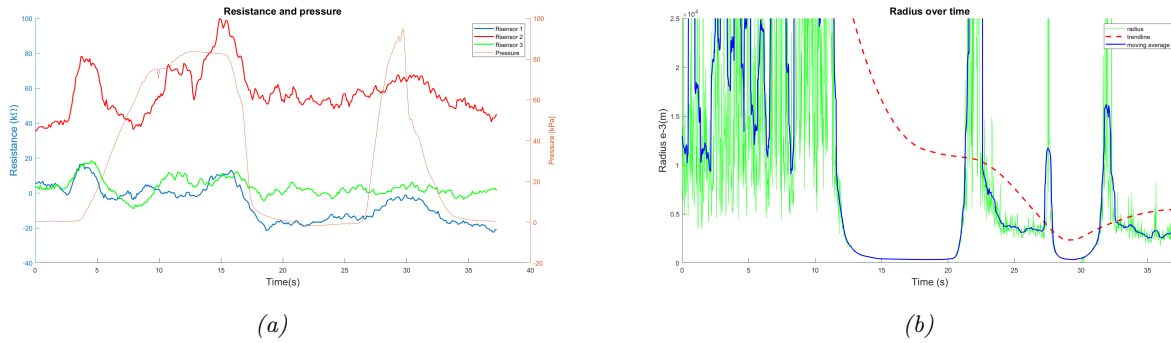


Figure 17: One chamber inflated, (a) Resistance and pressure over time, (b) radius over time

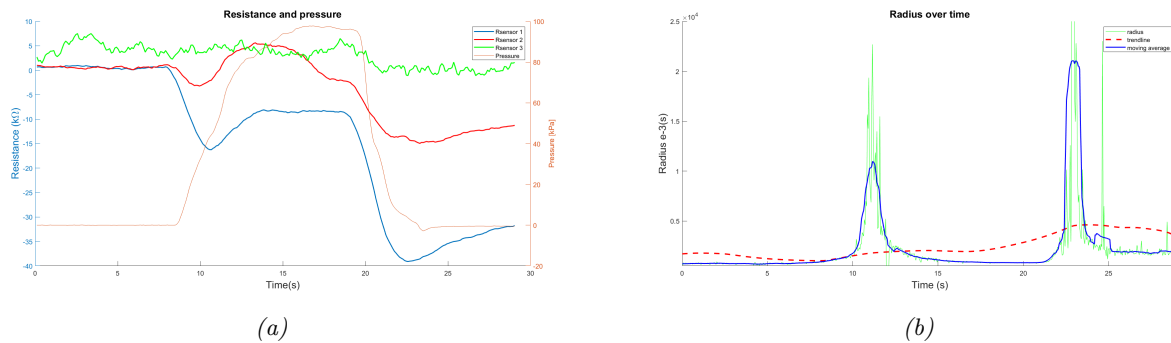


Figure 18: One chamber inflated, (a) Resistance and pressure over time, (b) radius over time

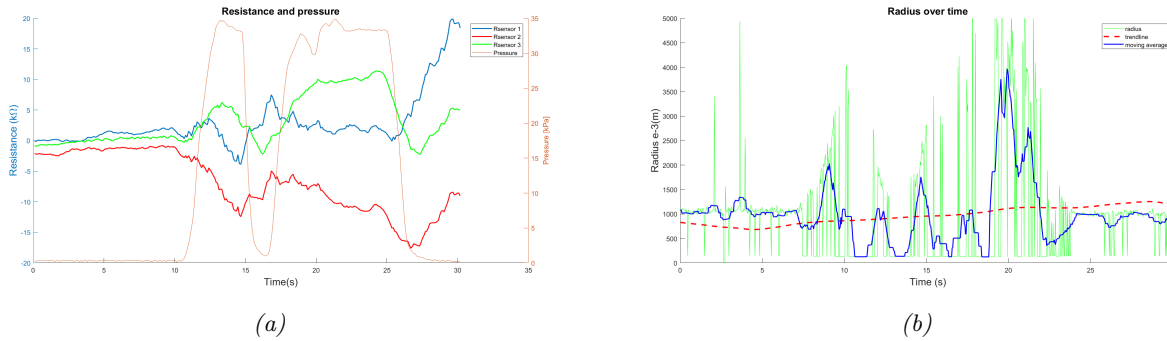


Figure 19: Two chambers inflated, (a) Resistance and pressure over time, (b) radius over time

Figure 17, 18, and 19 display the results of the sensor characterization. In the left Figure, the pressure and the moving average of the resistance over time are plotted. In Appendix Figures C.1, C.2, and C.3, the full signal is shown. In the right Figure the radius over time is plotted, also a trendline and a moving average are shown. The moving average has a window size of ten.

When looking at the results of the first video, Figures 16a and Figure 17. Firstly, it is visible that when the pressure increases the resistance of the sensors changes. All resistances start at a different point, but if looking at the absolute values, the resistance of sensor 1 has the biggest change. It is expected that sensors 1 and 2 show the biggest change. An illustration is in Figure 20, the left chamber is actuated, so the red and blue sensors are stretched the most.

The snapshot is made at 27 seconds, at this point pressure is added, displayed in Figure 17a. Likewise in Figure 17b it is visible that the radius is smaller here, which indicates a bent actuator. Furthermore in the period of five to 15 seconds when the pressure is high, the radius is small again indicating a bent actuator.

Figure 18 shows that the resistance of two sensors changes when pressure is added, sensor 3 almost does not respond. In Figure 18b two peaks are visible corresponding with the time when the pressure is added and released. The expected result would be a lower radius when the pressure is added, this is the case. However, the radius is also small in the first ten seconds and the last five seconds. In these time frames the actuator is in a straight configuration and thus a very high radius is expected.

It is expected that sensors 1 and 2 give the biggest resistance change, these sensors stretch the most in this configuration. These sensors have indeed the biggest resistance change. However sensor 1, blue, does have a bigger change than the red sensor. A reason for this can be that the actuator does not bend completely straight in between the sensors and the sensors are differently stretched. As well the sensors have a different start value, so their response

In Figure 16c and 19 the results of the sensor characterization when two chambers are inflated are shown. It is expected that the sensor in between the chambers will show the biggest resistance change, which is sensor 3 (green) in this case, this is illustrated in Figure 20. At ten seconds when the pressure is increased all sensors show a resistance change, the absolute change of sensor 2 is the biggest. When the actuator is inflated for the second time sensor 3 shows the biggest resistance change. Figure 19b does not show a clear radius difference when the actuator is inflated. A reason for this can be that the actuator has more than two black dots. The computer-vision can select multiple dots, which can change the radius. Moreover, the actuator does not bend that far, visible in Figure 16c. Consequently, the radius difference is a lot smaller compared to the other two videos.

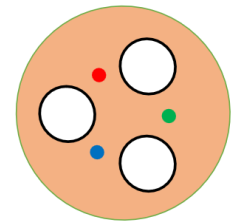


Figure 20: Upper sight of the module, with three highlighted sensors, sensor 1 blue, sensor 2 red, sensor 3 green.

In summary, when the actuator is inflated a resistance change is visible. The actuator can be followed and the radius can be calculated from the video. It is hard to determine in which way the actuator will be bent because in some cases all sensors show a resistance change. For almost all sensors applies that the resistance at the beginning of the measurement has a different value than when the measurement stops, while the actuator is in the same configuration. It could be possible the resistance needs more time to go to the beginning value again.

A lot of noise is visible in the radius over time Figures. To improve these results the videos could be made again to secure a better contrast. Besides, the lowest black dot should be placed higher, to secure more evenly spaced dots. In this computer-vision analysis, the lowest point is drawn by hand and this is close to the lowest black point. Secondly, it is visible all resistances start at a different value, a reason for this could be that the sensors

are thinner or thicker than the other. Moreover, a possibility is that the connection of some sensors is weaker. If this is improved the results will be better comparable. However, in the above results, a resistance change is visible. It could also be discussed how repeatable these experiments are. They cannot be repeated exactly, but if the goal is to see if there is a change in resistance and change in radius they are sufficient. Nevertheless to improve the experiment multiple modules can be made and tested multiple times. In this way also the repeatability of the results can be checked.

3.3 Sensor characterization full actuator

Figure 21 shows the actuator when both modules are inflated, the lower module bends a little so it is hard to see. Figure 22 shows the sensor results. Sensors 1.1, 1.2, and, 1.3 are from the lower module, the other sensors are from the top module. It is visible that when the actuator is moved, according to the protocol in Figure 11, the resistance of different sensors changes. It is visible that at 20 seconds the resistance of the sensors in the upper module changes, and the resistance of the lower module stays more constant. However, it is not visible which way the top module bends, because all sensors change. Notable is the high resistance change of sensor 1.3 at 40 seconds, the lower module is bent here, and the other two sensors of the module did not change resistance indicating sensor 1.3 is the sensor that is most stretched. When the actuator is put in an S-shape, which happens at 60 seconds, all resistances increase, and after that decrease slowly. From 70 seconds the actuator is in a straight configuration again and still the resistance decreases a bit.

This test is again hard to replicate, the bending is done by hand and can be different every time. Firstly this test can be improved by inflating the actuator instead of moving it by hand. Secondly, the test should be executed multiple times. Another suggestion is to make multiple actuators, to check if the resistance change is different between actuators. The experiment does show a resistance change when the actuator deforms. It can be determined which module, upper or lower is moving. However, it cannot be determined which way the module is bending.



Figure 21: Full actuator, both modules inflated

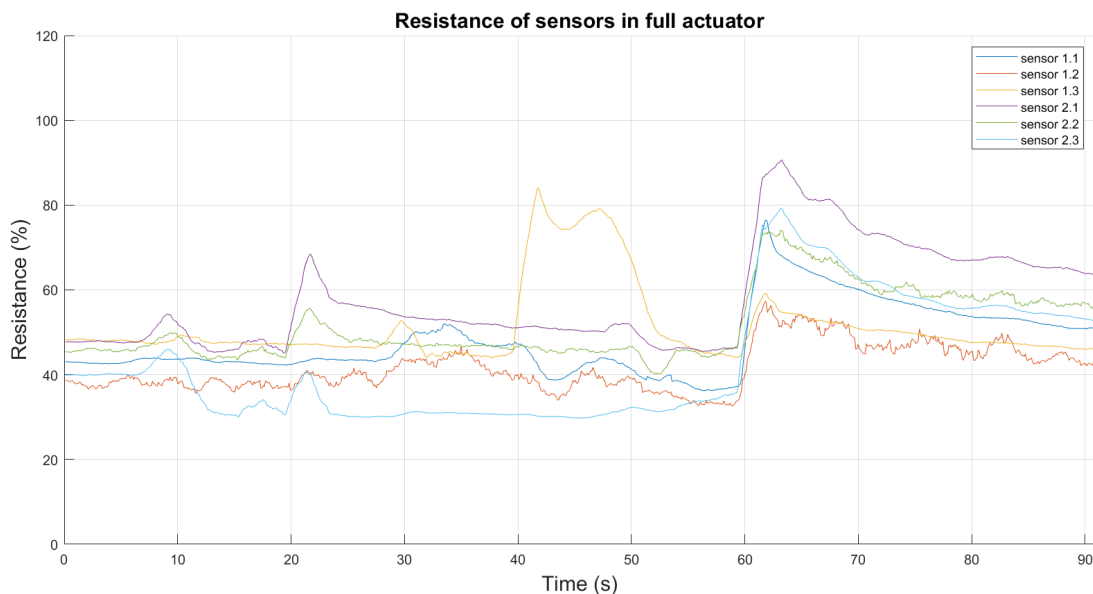


Figure 22: Resistance over time for all sensors in the actuator

4 Conclusion

The actuator is shown in Figure 23. It has a diameter of 35mm and a length of 160mm and is fabricated of Ecoflex 00-10. All connections are soldered and tubes are connected. The tubes have a diameter of 2mm , and the copper wires of 1mm . The copper wires in the middle ensure less elongation of the actuator. Without copper wires, the actuator would elongate more when the balloons are inflated. As a result of the copper wires, the actuator does not elongate but mainly bends when the balloons are inflated.

In clinical operations, endoscopes have a diameter of $5 - 10\text{mm}$ [24]. For future designs, it can be looked into making the actuator smaller. The limitation of this design is the size of the balloons, with the used device they cannot be made smaller. When redesigning the device, the balloons can be made smaller. Another way to improve the design is by increasing the pitch of the fiber reinforcements. In the current design sometimes balloons in the middle of the module appear, shown in Figure 24. Subsequently, if too much pressure is added the module ruptures, Figure 25. Moreover, the balloons can bend further when increasing the pitch. Wrapping the fiber in a different configuration can also be explored to achieve a higher bending angle.

Making fiber reinforced balloons is a time-consuming process. There are a lot of different steps and it needs to be done very precise. A way to improve the process is by making a mold for the balloon, curing silicon in this, and then wrapping fiber around it, this is done by Fras et al. [25]. It will make sure every balloon is the same size, moreover, it is possible to make them smaller.

Another way to improve the design, and make it easier to fabricate the module, is to think about a way to add the tubes when the whole module is made. The tubes could for example be added in the step of Figure A.5. The method that is used in this study often causes leakages or balloons forming where the tube is connected. Also, there can be thought about putting some stronger silicon rubber at the top of the actuators instead of Ecoflex 00-10. This will make sure no bubbles will form at the top of the actuator.

To improve the results of the sensors first, it needs to make sure every sensor has the same resistance at the beginning. This can be tested before the sensors are implemented. Secondly, the tests should be more repeatable. Thirdly, more tests should be executed to be able to determine the bending angle of the actuator according to the resistance data.

In the introduction, the future possibilities of soft endoscopes are described and visualized in Figure 2. This study contributes to the first step in designing a soft sensory actuator and gaining insight into the sensor characterization of such an actuator. Different sensors are explored and conductive rubber was further used. The tests showed that when the actuator bends and the sensor stretches the resistance changes. Figure 26 shows an example of a joystick that was designed by a fellow student. The joystick is 3D printed and also consists of two parts, to be able to form an S-shape. When further developed the actuator and joystick may be connected to control the actuator with the joystick.



Figure 23: Final actuator



Figure 24: Module with bubble



Figure 25: Ruptured module



Figure 26: Joystick to control an actuator

Bibliography

- [1] Robinson TN, Stiegmann GV. Minimally invasive surgery. *Endoscopy*. 2004 Jan;36(1):48-51. doi:10.1055/s-2004-814113.
- [2] Azar FM. Minimally Invasive Surgery: Is Less More? *Orthop Clin North Am*. 2020 Jul;51(3):xiii-xiv. doi:10.1016/j.ocl.2020.04.001.
- [3] Mattingly AS, Chen MM, Divi V, Holsinger FC, Saraswathula A. Minimally Invasive Surgery in the United States, 2022: Understanding Its Value Using New Datasets. *J Surg Res*. 2023 Jan;281:33. doi:10.1016/j.jss.2022.08.006.
- [4] Marieke J Krimphove #, Stephen W Reese #, Chen X, Marchese M, Pucheril D, Cone E, et al. Recovery from minimally invasive vs. open surgery in kidney cancer patients: Opioid use and workplace absenteeism. *Investig Clin Urol*. 2021 Jan;62(1):56-64. doi:10.4111/icu.20200194.
- [5] Fan CJ, Chien HL, Weiss MJ, He J, Wolfgang CL, Cameron JL, et al. Minimally invasive versus open surgery in the Medicare population: a comparison of post-operative and economic outcomes. *Surg Endosc*. 2018 Sep;32(9):3874-80. doi:10.1007/s00464-018-6126-z.
- [6] Searle TC, Althoefer K, Seneviratne L, Liu H. An optical curvature sensor for flexible manipulators. Published in: 2013 IEEE International Conference on Robotics and Automation:06-10. doi:10.1109/ICRA.2013.6631203.
- [7] Abidi H, Gerboni G, Brancadoro M, Frasc J, Diodato A, Cianchetti M, et al. Highly dexterous 2-module soft robot for intra-organ navigation in minimally invasive surgery. *Int J Med Rob Comput Assisted Surg*. 2018 Feb;14(1):e1875. doi:10.1002/rcs.1875.
- [8] Loeve A, Breedveld P, Dankelman J. Scopes Too Flexible...and Too Stiff. *IEEE Pulse*. 2010 Nov;1(3):26-41. doi:10.1109/MPUL.2010.939176.
- [9] Morino M, Parini U, Giraud G, Salvati M, Brachet Contul R, Garrone C. Laparoscopic Total Mesorectal Excision: A Consecutive Series of 100 Patients. *Ann Surg*. 2003 Mar;237(3):335. doi:10.1097/01.SLA.0000055270.48242.D2.
- [10] Stilli A, Wurdemann H, Althoefer K. Shrinkable, stiffness-controllable soft manipulator based on a bio-inspired antagonistic actuation principle. 2014 IEEE/RSJ International Conference on Intelligent Robots and Systems. 2014.
- [11] Mosadegh B, Polygerinos P, Keplinger C, Wennstedt S, Shepherd RF, Gupta U, et al. Pneumatic Networks for Soft Robotics that Actuate Rapidly. *Adv Funct Mater*. 2014 Apr;24(15):2163-70. doi:10.1002/adfm.201303288.
- [12] Fiber-Reinforced Actuators. Soft robotics toolkit. Available from: <https://softroboticstoolkit.com/book/fr-variation-motion>.
- [13] Shepherd RF, Ilievski F, Choi W, Morin SA, Stokes AA, Mazzeo AD, et al. Multigait soft robot. *Proc Natl Acad Sci USA*. 2011 Dec;108(51):20400-3. doi:10.1073/pnas.1116564108.
- [14] Maeder-York P, Clites T, Boggs E, Neff R, Walsh C. Biologically Inspired Soft Robot for Thumb Rehabilitation1. *J Med Devices*. 2014 Jun;8(2):020934. doi:10.1115/1.4027031.
- [15] Connolly F, Walsh CJ, Bertoldi K. Automatic design of fiber-reinforced soft actuators for trajectory matching. *Proc Natl Acad Sci USA*. 2017 Jan;114(1):51-6. doi:10.1073/pnas.1615140114.
- [16] Cianchetti M, Ranzani T, Gerboni G, Falco ID, Laschi C, Menciassi A. STIFF-FLOP surgical manipulator: Mechanical design and experimental characterization of the single module. 2013 IEEE/RSJ International Conference on Intelligent Robots and Systems. 2013.
- [17] Fraś J, Czarnowski J, Maciąs M, Głównka J, Cianchetti M, Menciassi A. New STIFF-FLOP module construction idea for improved actuation and sensing. Published in: 2015 IEEE International Conference on Robotics and Automation (ICRA):26-30. doi:10.1109/ICRA.2015.7139595.

-
- [18] Amjadi M, Kyung KU, Park I, Sitti M. Stretchable, Skin-Mountable, and Wearable Strain Sensors and Their Potential Applications: A Review. *Advanced Functional Materials*. 2016;26(11):1678-98. doi:10.1002/adfm.201504755.
- [19] Noh Y, Secco EL, Sareh S, Wurdemann H, Faragasso A, Back J, et al. A continuum body force sensor designed for flexible surgical robotics devices. *Annu Int Conf IEEE Eng Med Biol Soc*. 2014;2014:3711-4.(;):Annu. doi:10.1109/EMBC.2014.6944429.
- [20] Truby RL, Santina CD, Rus D. Distributed Proprioception of 3D Configuration in Soft, Sensorized Robots via Deep Learning. *IEEE Rob Autom Lett*. 2020 Feb;5(2):3299-306. doi:10.1109/LRA.2020.2976320.
- [21] Ata S, Kobashi K, Yumura M, Hata K. Mechanically Durable and Highly Conductive Elastomeric Composites from Long Single-Walled Carbon Nanotubes Mimicking the Chain Structure of Polymers. *Nano Lett*. 2012 Jun;12(6):2710-6. doi:10.1021/nl204221y.
- [22] Sekitani T, Noguchi Y, Hata K, Fukushima T, Aida T, Someya T. A rubberlike stretchable active matrix using elastic conductors. *Science*. 2008;321. doi:10.1126/science.1160309.
- [23] Shin MK, Oh J, Lima M, Kozlov ME, Kim SJ, Baughman RH. Elastomeric Conductive Composites Based on Carbon Nanotube Forests. *Adv Mater*. 2010 Jun;22(24):2663-7. doi:10.1002/adma.200904270.
- [24] Structure and Components of Endoscopes. Olympus-global. Available from: https://www.olympus-global.com/ir/data/pdf/ir_medical_2022e_08.pdf.
- [25] Fras J, Macias M, Czarnowski J, Brancadoro M, Menciassi A, Glowka J. Soft Manipulator. In: *Soft and Stiffness-controllable Robotics Solutions for Minimally Invasive Surgery*. Upper Saddle River, NJ, USA: River Publishers; 2022. p. 47-63. doi:10.1201/9781003339588-4.

List of Figures

1	Illustration of a soft device and a rigid instrument in the human body [7]	3
2	Vizualization of future application	3
3	PneuNet actuator [11]	4
4	Illustration of different configurations of the strain-limiting components [12]	4
5	STIFF FLOP design [16]	4
6	Prototype visualization in Solidworks, all dimensions in mm	5
7	Mold to make the actuator	5
8	Overview of the fabrication process	5
9	(a) circuit diagram of a voltage divider, (b) setup for testing conductive rubber, (c) setup for testing water with salt, (d) example of the bending angle	7
10	Schematic setup of the video analysis	7
11	Protocol to test the sensorized actuator, time in seconds.	8
12	Test results water and salt 100g/L, (a) Straight and bend, (b) Straight and straight stretched, (c) Bend and bend stretched, (d) Straight stretched and bend stretched	9
13	Test results water and salt 200g/L, (a) Straight and bend, (b) Straight and straight stretched, (c) Bend and bend stretched, (d) Straight stretched and bend stretched	10
14	Test results conductive rubber, (a) Straight and bend, (b) Straight and straight stretched, (c) Bend and bend stretched, (d) Straight stretched and bend stretched	11
15	Test results straight sensor for 500 seconds, (a) Conductive rubber, (b) Water and salt 100g/L, (c) Water and salt 200g/L	12
16	Snapshot of the video where maximum bending is reached (a) at 27 seconds, (b) at 15 seconds, (c) at 10 seconds	13
17	One chamber inflated, (a) Resistance and pressure over time, (b) radius over time	13
18	One chamber inflated, (a) Resistance and pressure over time, (b) radius over time	13
19	Two chambers inflated, (a) Resistance and pressure over time, (b) radius over time	14
20	Upper sight of the module, with three highlighted sensors, sensor 1 blue, sensor 2 red, sensor 3 green.	14
21	Full actuator, both modules inflated	15
22	Resistance over time for all sensors in the actuator	15
23	Final actuator	16
24	Module with bubble	16
25	Ruptured module	16
26	Joystick to control an actuator	17
A.1	Left: Fiber reinforced balloon, Right: Balloon without fiber	21
A.2	Tool to wrap the fiber around silicon balloon.	21
A.3	Mold design in Solidworks	21
A.4	Mold to connect two modules	22
A.5	Mold with balloons and pins, before adding silicon.	22
A.6	One module	22
A.7	Setup for the video analysis	22
B.1	First mold with balloons and pins	23
B.2	SolidWorks design first mold	23
B.3	First prototype, not enough silicon	23
C.1	Resistance and pressure over time, one chamber	23
C.2	Resistance and pressure over time, one chamber	24
C.3	Resistance and pressure over time, two chambers	24

Appendix

A Extra figures fabrication and setup

In this section, some extra pictures and figures are added. Figure A.1 shows a fiber reinforced balloon and a balloon before the fibers are wrapped around it. Figure A.2 shows the tool that is used to wrap the fibers around. Some extra pictures of the mold for the actuator are shown in Figure A.3 and in Figure A.4 the mold to connect two modules is shown. Figure A.5 shows the mold with balloons and pins before silicon is added. The result of this is shown in Figure A.6, here also the plastic tubes are connected. A picture of the setup for the video analysis is shown in Figure A.7. The syringe is secured in Lego blocks, which are secured on the working station. A white plate is used as a background to secure a good contrast with the black dots. The module is placed in a plastic mold in a vice. The camera is placed on a tripod. The wires and Arduino are covered with a blue cloth.



Figure A.1: Left: Fiber reinforced balloon,
Right: Balloon without fiber

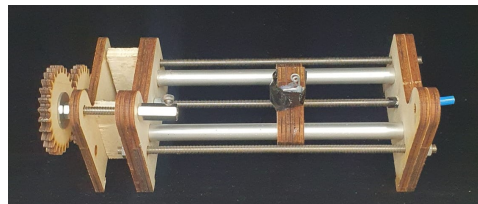
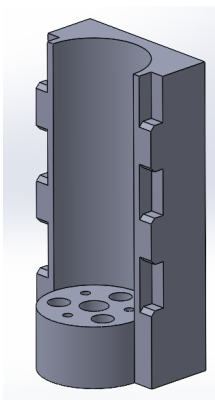
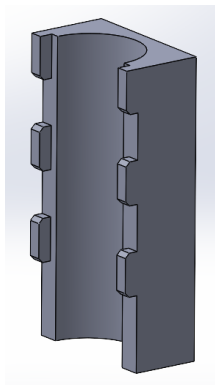


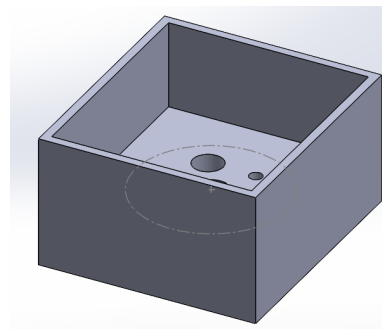
Figure A.2: Tool to wrap the fiber around silicon balloon.



(a) Mold, part A



(b) Mold, part B



(c) Mold, cap

Figure A.3: Mold design in Solidworks

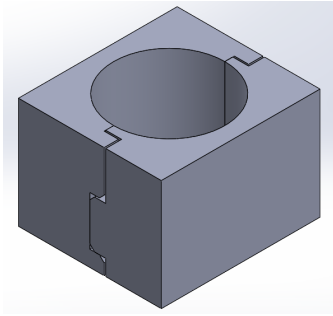


Figure A.4: Mold to connect two modules

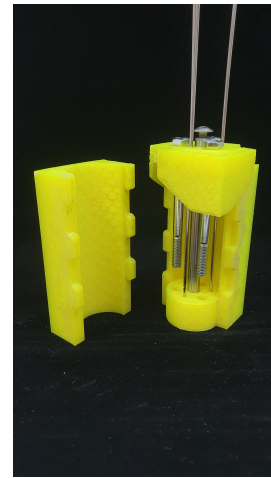


Figure A.5: Mold with balloons and pins, before adding silicon.



Figure A.6: One module

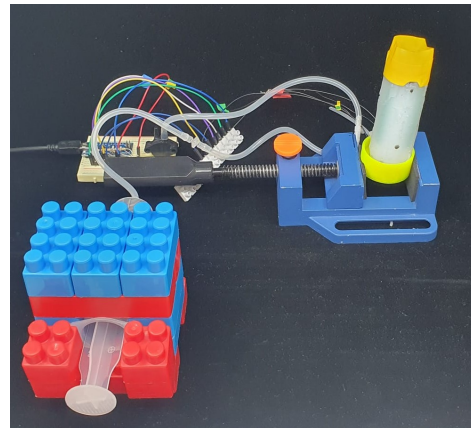


Figure A.7: Setup for the video analysis

B First mold design

The first mold that was created is seen in Figure B.1 and the SolidWorks design in Figure B.2. The prototype from this mold is seen in Figure B.3. It was hard to get the prototype out of the mold. So for the new mold design, two parts were made to make it easier to get the actuator out of the mold.

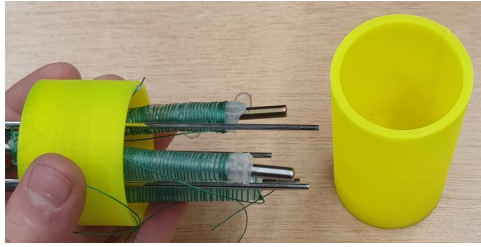


Figure B.1: First mold with balloons and pins

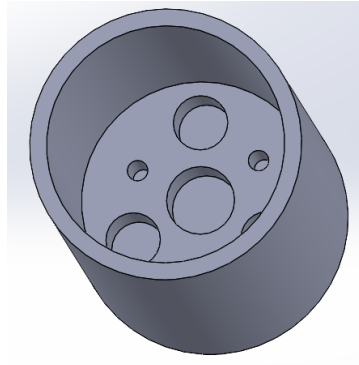


Figure B.2: SolidWorks design first mold



Figure B.3: First prototype, not enough silicon

C Results resistance and pressure over time

Figure C.1, C.2 and C.3 show the resistance and pressure over time. The resistance and the moving average of each sensor are plotted.

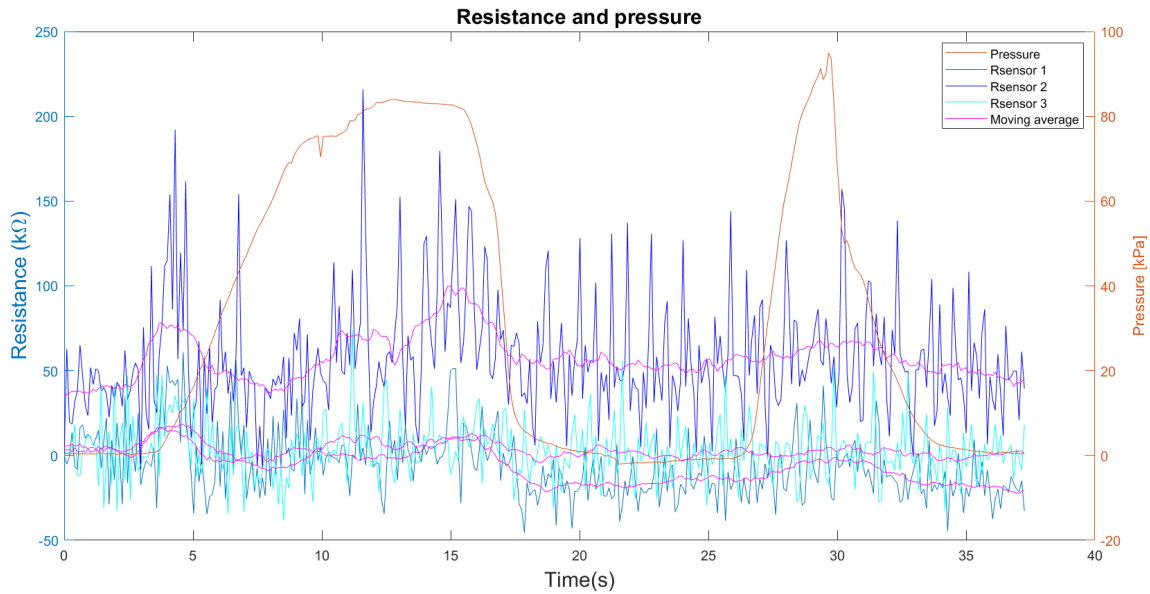


Figure C.1: Resistance and pressure over time, one chamber

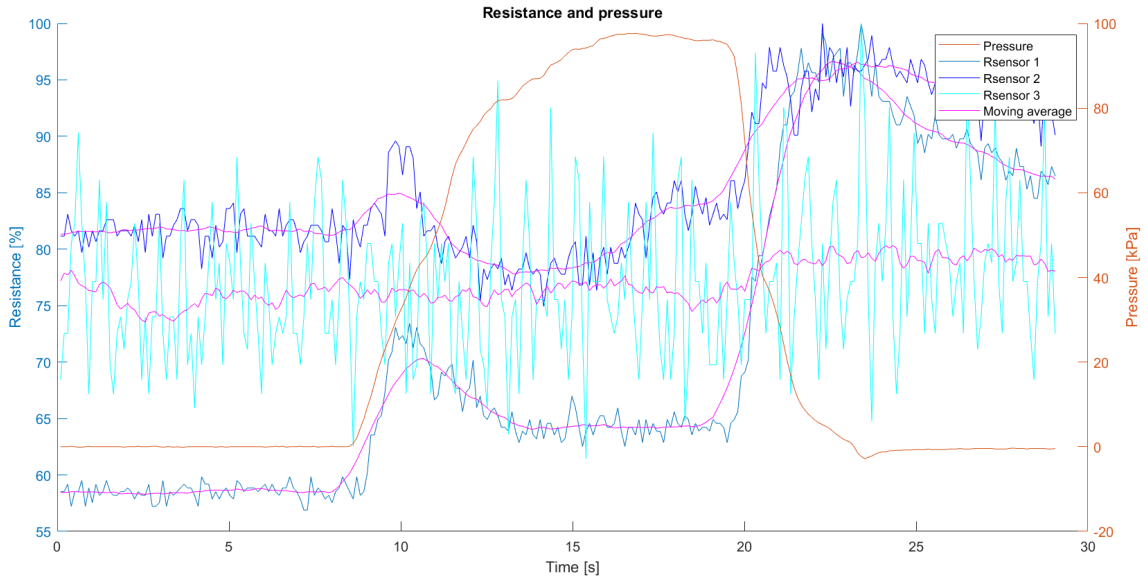


Figure C.2: Resistance and pressure over time, one chamber

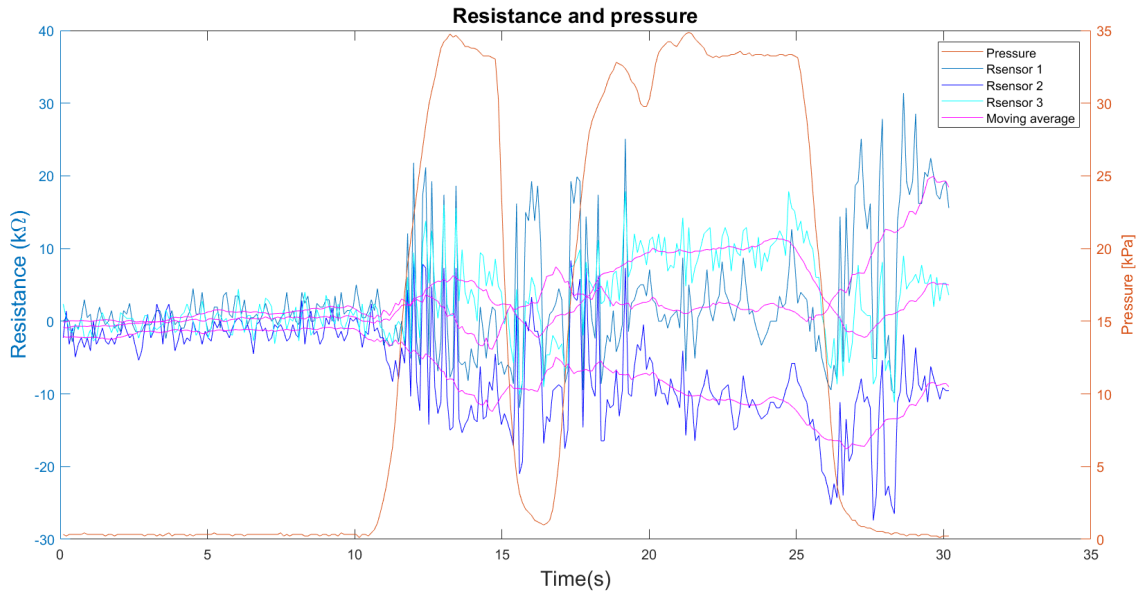


Figure C.3: Resistance and pressure over time, two chambers